

THE OFFICIAL MAGAZINE OF THE OCEANOGRAPHY SOCIETY

Oceanography

CITATION

Smyth, W.D., and J.N. Moum. 2012. Ocean mixing by Kelvin-Helmholtz instability. *Oceanography* 25(2):140–149, <http://dx.doi.org/10.5670/oceanog.2012.49>.

DOI

<http://dx.doi.org/10.5670/oceanog.2012.49>

COPYRIGHT

This article has been published in *Oceanography*, Volume 25, Number 2, a quarterly journal of The Oceanography Society. Copyright 2012 by The Oceanography Society. All rights reserved.

USAGE

Permission is granted to copy this article for use in teaching and research. Republication, systematic reproduction, or collective redistribution of any portion of this article by photocopy machine, reposting, or other means is permitted only with the approval of The Oceanography Society. Send all correspondence to: info@tos.org or The Oceanography Society, PO Box 1931, Rockville, MD 20849-1931, USA.

Ocean Mixing by Kelvin-Helmholtz Instability

BY WILLIAM D. SMYTH AND JAMES N. MOUM

ABSTRACT. Kelvin-Helmholtz (KH) instability, characterized by the distinctive finite-amplitude billows it generates, is an important mechanism in the development of turbulence in the stratified interior of the ocean. In particular, it is often assumed that the onset of turbulence in internal waves begins in this way. Clear recognition of the importance of KH instability to ocean mixing arises from recent observations of the phenomenon in a broad range of oceanic environments. KH instability is a critical link in the chain of events that leads from internal waves to mixing. After 150 years of research, identifying the prevalence of KH instability in the ocean and defining useful parameterizations that quantify its contribution to ocean mixing in numerical models remain first-order problems.

INTRODUCTION

A regime of strongly nonlinear fluid motions exists at scales smaller than can be resolved by global ocean models. They include a broad range of phenomena that exhaust at least some of their energy to turbulence. While these organized motions are generally well understood, there is as yet no deterministic theory for the resulting turbulence. In practice, we understand turbulence through the statistics of its density, velocity, and vorticity fluctuations. Turbulence stirs the ocean, stretching material surfaces and locally increasing gradients to the point

that they rapidly and irreversibly diffuse at molecular scales. This process is ultimately responsible for mixing the ocean.

The transition from organized flow to turbulence occurs through a sequence of instability processes, beginning with a primary instability. Different primary instabilities dominate under different circumstances. For example, cooling of the sea surface generates cool (and therefore dense) fluid parcels that sink once buoyant forces exceed viscous forces. This is one form of convective instability. The resulting turbulence acts to homogenize the ocean's surface layer, particularly

at night. Another form of convective instability (sometimes called "advective" instability) occurs in gravity waves when the particle motion exceeds the wave speed, such as in a breaking surface wave. Some parts of the ocean are mixed by double-diffusive instabilities due to the combined effects of temperature and salinity on the density of seawater.

In the stratified interior, mixing is most often mediated by internal waves, whose energy comes from a combination of wind and tidal forcing. Internal wave shear (vertical gradient of horizontal velocity) counters the stabilizing effect of density stratification and can generate primary instability of the Kelvin-Helmholtz (KH) type. The tendency for instability to grow despite the damping action of stable stratification is quantified using the gradient Richardson number (Ri , the ratio of the squared buoyancy frequency to the squared vertical shear of the horizontal flow). When shear is strong enough (or stratification weak enough) to bring Ri below a critical



Figure 1. Kelvin-Helmholtz billows revealed by clouds. (a) Side view (from <http://www-frd.fsl.noaa.gov/mab/scatcat>; photo by Brooks Martner). (b) Kelvin-Helmholtz billows made visible by a fog layer on the shore of Nares Strait in the Canadian Arctic (courtesy of Scott McAuliffe, Oregon State University). (c) Ground view of billow clouds (<http://www.weathervortex.com/sky-ribbons.htm>), showing large-scale knot instabilities (Thorpe, 2002) and thin striations consistent with convection rolls (Klaassen and Peltier, 1991).

value, instability is possible. The result is a growing wave train reminiscent of surface waves approaching a beach (e.g., atmospheric examples shown in Figures 1a,b, 2, 3, and 4). The maximum shear primarily determines the instability's growth rate, while wavelength is typically an order of magnitude greater than the thickness of the sheared layer.

Visual evidence for KH instability frequently can be seen at the top of the atmospheric boundary layer in late afternoon and evening, where it appears as patches of banded clouds (occasionally seen in Web videos of flows near Marys Peak taken from the top of our building at Oregon State University and shared at <http://marycam.coas.oregonstate.edu>). Seen from the side, such clouds often take shapes similar to those of surface waves breaking on a beach. Figure 1 shows vivid examples from the atmosphere and from a low-level shear flow in the Canadian Arctic. Increasingly high-fidelity ocean measurements have led to

William D. Smyth (smyth@coas.oregonstate.edu) and **James N. Moum** are professors in the College of Earth, Ocean and Atmospheric Sciences, Oregon State University, Corvallis, Oregon, USA.

clear observations of the presence and structure of KH billows in the ocean.

In this article, we review the history and current status of research into KH instability with a focus on its role in the energy cascade from oceanic internal waves to small-scale turbulence.

SOME HISTORY

Named in honor of the pioneering investigators William Thomson (Lord Kelvin, 1824–1907) of Glasgow and Hermann von Helmholtz (1821–1894) of Berlin, “Kelvin-Helmholtz instability” referred originally to the instability of two adjacent fluid layers in relative motion. Thomson (1871) used this instability as a model for the generation of ocean surface waves by wind, while von Helmholtz (1890) sought to explain the banded clouds discussed above. In real fluids, a transition layer of nonzero thickness—a shear layer—always separates the layers.

Disturbances between moving fluid layers were first documented via experiments in a tilting tube by Reynolds (1883)¹. In these experiments, a long horizontal tube containing two fluid layers of different densities was tipped

slightly, so that the buoyancy difference set the layers in motion relative to one another, resulting in the formation of waves at the interface. Thorpe (1971; Figure 2) documented the large-amplitude, two-dimensional structure in which vorticity creates billows and intermingles the fluids from adjacent layers.

Theoretical studies of the homogeneous shear layer by Lord Rayleigh (1880) were extended to include the effects of stable density stratification by Taylor (1927, 1931), who also demonstrated stratification effects in the laboratory, and Goldstein (1931). The equation that describes the instability in the absence of viscosity and diffusion is called the Taylor-Goldstein equation in their honor (Thorpe, 1969). Miles (1961) and Howard (1961) showed the critical value of Ri to be $\frac{1}{4}$.

The occurrence of KH billows in the ocean was first revealed when scuba divers conducted dye-release experiments in the stratified thermocline of the Mediterranean Sea (Woods, 1968, shown here in Figure 3). Photographs of the resulting dye patterns revealed billow trains associated with internal

¹ They were part of a series of fluid experiments performed by Reynolds on the transition to turbulence from which the *Reynolds number* was first defined.

gravity waves (IGWs) of much greater wavelength, as well as small-scale streaks suggestive of secondary instability (Figure 3b). The spatial and temporal scales of the billows compared favorably with predictions based on the theory of KH instability. The photos also showed the role of KH billows in IGW breaking as, following the instability, the dye quickly mixed away.

Hazel (1972) constructed numerical solutions of the Taylor-Goldstein equation for a number of idealized velocity and density profiles that have proven useful in modeling naturally occurring stratified shear flows. One of them was a shear layer in which velocity and density varied continuously between two

homogeneous layers. All models of shear layers (both laboratory and theoretical) generate instability and vortex rollup if Ri is small enough. Today, this class of processes is referred to in general as “Kelvin-Helmholtz instability.”

The importance of KH instability has been documented observationally in a variety of oceanic regimes, for example, within strongly sheared estuarine flows (Geyer and Smith, 1987; Geyer et al., 2010) and at the edges of gravity currents (Wesson and Gregg, 1994). Van Haren and Gostiaux (2010; Figure 4) have observed a train of about 10 billows in a highly sheared zone associated with tidal flow at 560 m depth over Great Meteor Seamount.

KH INSTABILITY AND INTERNAL WAVE BREAKING

In uniform stratification (a useful approximation for the main thermocline), shear instability is dominant in waves of near-inertial frequency, where motions are nearly parallel and primarily horizontal. This is true even when wave amplitude is large enough that isopycnals are overturned (Dunkerton 1997; Lelong and Dunkerton, 1998a,b). (However, instability differs from the standard KH model in that the mean flow structure is a sinusoid rather than a shear layer.) Higher-frequency waves are more likely to break via convective instability. Internal waves in the thermocline may also break via parametric subharmonic instability (e.g., Hibiya et al., 1998), or by a resonance with small-scale instability such as salt fingering (Stern, 1969).

Nonlinear interfacial waves, as may occur at the base of a surface mixed layer, break primarily via KH instability (e.g., Moum et al., 2003; Lamb and Farmer, 2011). Internal waves encountering topography have been found to break via KH instability in the boundary layer and via convective instability in the interior (Venayagamoorthy and

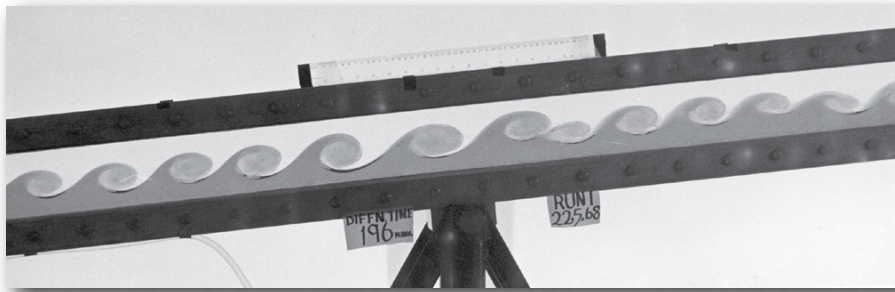


Figure 2. Tilting tank laboratory experiment in which a dense (here, dark) layer of fluid underlies a lighter fluid initially at rest. When the tank is tilted, buoyant forces accelerate the denser fluid down and the lighter fluid up the slope, thereby creating a velocity gradient across the interface and subsequent billow formation (Thorpe, 1971).

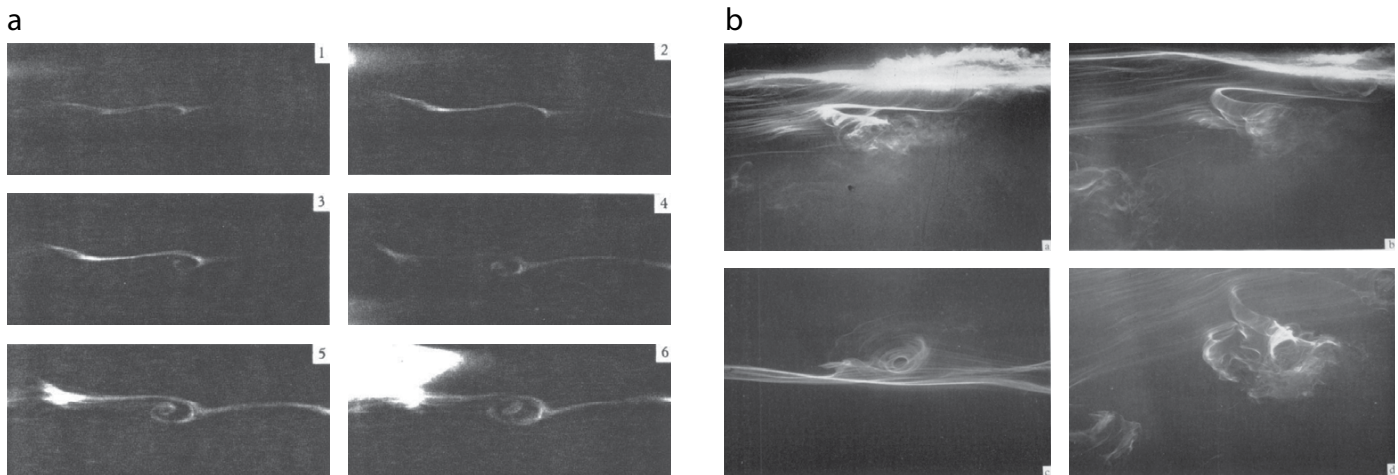


Figure 3. Underwater snapshots made by divers from laboriously executed dye release experiments in the Mediterranean thermocline (Woods, 1968). (a) Side view of the rollup of a Kelvin-Helmholtz billow. (b) Shear instabilities viewed in the context of larger-scale waves.

Fringer, 2012, in this issue).

Many classes of ocean models implicitly assume mixing via shear instability by applying mixing in regimes of low Ri , for example, the one-dimensional mixed layer models of Mellor and Yamada (1982) and Price et al. (1986). The Gregg-Henyey-Polzin scaling of dissipation due to fine-scale internal wave interactions (Henyey et al., 1986; Gregg, 1989; Polzin et al., 1995) rests on a similar assumption. A direct connection between turbulence and low Ri in the North Atlantic thermocline has provided quantitative evidence for the prevalence of shear instability (Polzin, 1996).

MECHANICS OF THE ENERGY CASCADE

The tendency of vorticity in a parallel shear layer to accumulate into evenly spaced maxima is the primary driver of KH instability. Given an initial wavelike perturbation, mass conservation requires accelerated horizontal flow above the crests and below the troughs (Figure 5a). The resulting current anomalies advect vorticity toward the center of the figure. The vorticity concentration induces vertical velocity perturbations that amplify the original wave (Figure 5b), resulting in positive feedback and exponential growth of the perturbation.² The most-amplified wavelength depends on the details of the initial profiles, but typically ranges from 6 to 11 times the initial transition-layer thickness. Stable stratification tends to slow the growth of the billows, but also to accelerate breaking once the billows reach sufficient amplitude to overturn. Internal waves in the ocean contain regions of strong

shear and stratification that are well described by this scenario, particularly in cases where two or more wave trains interfere constructively.

The downscale energy cascade from IGW to turbulence often begins with KH instability, but it does not end there. We can identify at least one further step, that being one of several secondary instabilities that grow on mature KH billows. The classic review article of Thorpe (1987) describes several such instabilities; today, several more are known. To compute these secondary instabilities, a two-dimensional KH billow is first simulated numerically. Further analysis then determines which *three-dimensional* perturbation, if applied to the finite-amplitude billow, would grow most rapidly (e.g., Klaassen and Peltier 1985, 1991).

This perturbation is identified as a secondary instability. In the example given in Figure 6, the secondary instability is represented by its vorticity field, which describes a series of counter-rotating convection cells in regions of the core where the density field is overturned. Similar motions have been seen in laboratory experiments (e.g., Thorpe 1985), in the ocean (Figure 3b), and in clouds (Figure 1c). Other examples include the secondary KH instability (Corcos and Sherman, 1976; Staquet, 1995; Smyth, 2003; Figure 7d), the “knot” instability that causes localized pairing (Thorpe 1985, 2002; Figure 1c), and the “stagnation point” instability of Mashayek and Peltier (2011). The latter may explain the form of KH billows observed in the Connecticut River estuary (Geyer et al.,

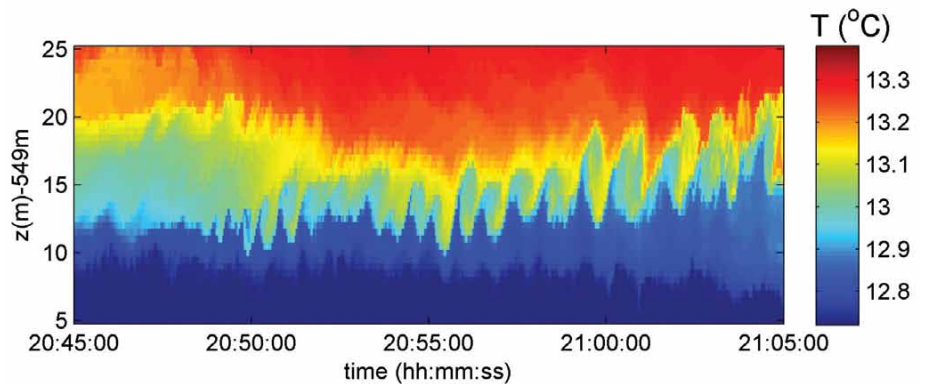


Figure 4. Temperature variations in a downslope tidal flow (van Haren and Gostiaux, 2010). This time series was constructed using data from multiple temperature sensors spaced vertically on a chain above the seafloor at 550 m depth. Typical wavelengths are inferred to be 75 m. Graphic courtesy H. van Haren

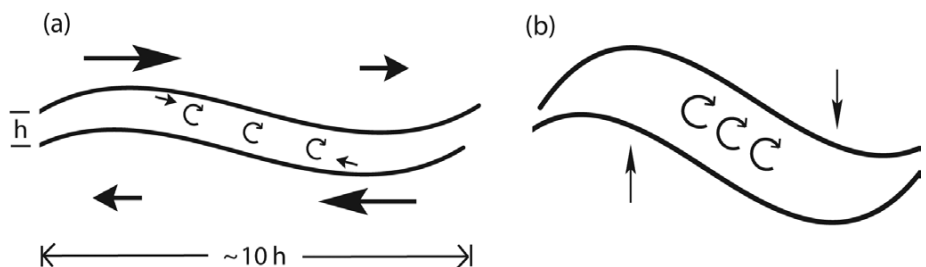


Figure 5. Schematic representation of the positive feedback that drives shear instability. (a) Vorticity accumulation due to horizontal advection. (b) Amplification of the initial wave by induced vertical motions.

² A more modern view of shear-driven instabilities is phrased in terms of resonances between vorticity and gravity waves (e.g., Baines and Mitsudera, 1994).

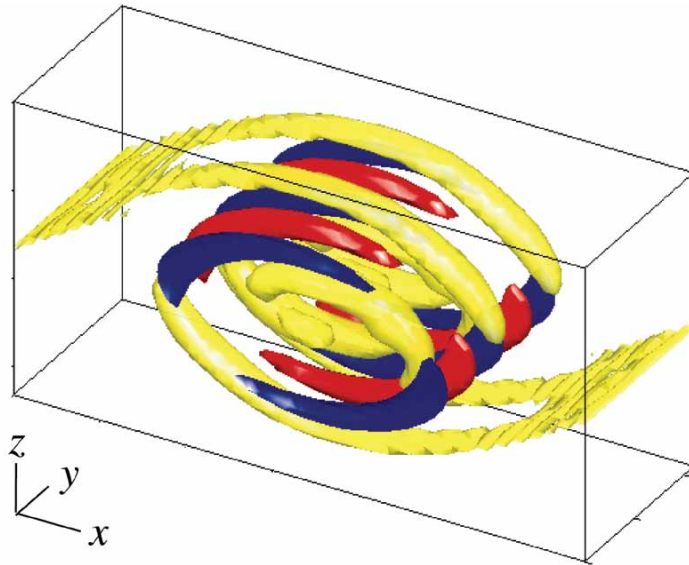


Figure 6. Secondary instability of a Kelvin-Helmholtz billow calculated using perturbation analysis. Colors show the perturbation vorticity field. Yellow indicates perturbations of the spanwise (y) vorticity that defines the primary instability. Red and blue show opposite signs of the streamwise (x) vorticity.

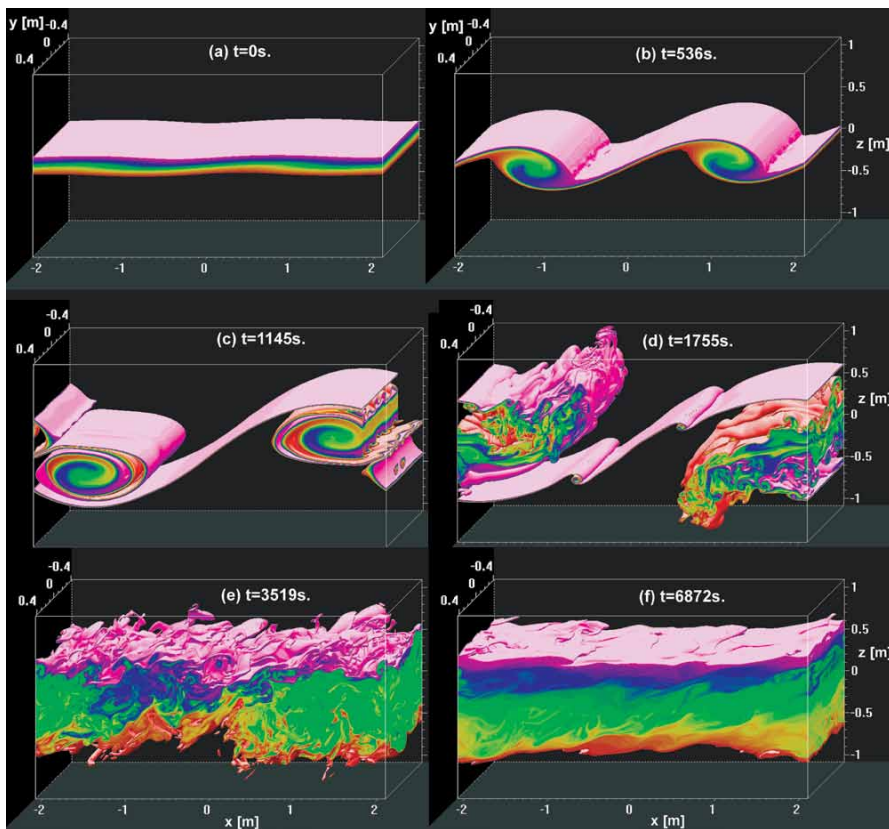


Figure 7. Direct numerical simulations of the density field at successive time in the life cycle of a Kelvin-Helmholtz billow train. Colors show density in the transition layer; upper and lower homogeneous layers are rendered transparent. (a) The initial state is a two-layer flow, with a lower (dense) layer flowing to the left and an upper layer to the right. A small perturbation is applied. (b) Two wavelengths of the primary Kelvin-Helmholtz instability. (c) Kelvin-Helmholtz billows are beginning to pair. Secondary instability is visible in a cutaway at upper right, taking the form of shear-aligned convection rolls. (d) Secondary shear instability forms on the braids. (e) The fully turbulent state. (f) Turbulence decays to form sharp layers and random small-scale waves.

2010) and on the Oregon continental shelf (Moum et al., 2003, shown in Figure 8). The question of which secondary instabilities are most important for the development of turbulence in oceanic billows remains unresolved. While complex, these secondary instabilities are not turbulent, so further transitions (i.e., tertiary instabilities and beyond) must be present.

EVOLUTION OF THE INSTABILITY IN NUMERICAL SIMULATIONS

With recent increases in computational power, it has become feasible to study the energy cascade via direct simulation of the full three-dimensional dynamics. Through direct numerical simulations, we are uniquely able to examine in detail the full evolutionary cycle of flow instabilities. Simulations are limited by available computer memory and, therefore, cannot fully replicate the range of interactions that occur in geophysical flows. However, with full resolution of the smallest scales, they reveal both the nonlinear evolution of the primary instability and the sequence of secondary instabilities that leads to turbulence. Moreover, simulations furnish a quantitative representation of the resulting turbulence and the mixing it causes.

The first numerical simulations of KH instability were restricted to two dimensions due to memory limitations (e.g., Patnaik et al., 1976; Klaassen and Peltier, 1985). These simulations confirmed the primary instability but could not resolve the subsequent transition to three-dimensional motion. Three-dimensional simulations became possible in the 1990s (Caulfield and Peltier, 1994; Scinocca, 1995) and have been used in numerous studies since then as

computational capacity has increased. Early numerical studies assumed that momentum and mass diffuse at the same rate, as is approximately true in air. Increasing computer size has also allowed simulations of instability in seawater, which is more difficult due to the slow diffusion rates of heat and salt (Smyth, 1999; Kimura and Smyth, 2007; Smyth and Kimura, 2011).

In the example shown in Figure 7, the diffusivities are characteristic of thermally stratified seawater (see Smyth and Thorpe, 2012, for further details). Figure 7a shows the initial state—two layers separated by a thin transition layer. A small perturbation grows to form a train of KH billows, two of which are shown in Figure 7b. The billows subsequently merge and develop two secondary instabilities in sequence: convective secondary instability in overturned regions of the billow cores (Figure 7c, cf. Figure 6) and secondary shear instability in the braids (Figure 7d). These instabilities, and a complex combination of tertiary instabilities, lead the flow to a fully turbulent state (Figure 7e). Ultimately, turbulence decays, leaving a field of random IGWs propagating on a layer that has been dramatically thickened by irreversible mixing (Figure 7f, compare with 7a). The statistical properties of simulated mixing events like those shown here closely resemble those extracted from observations of turbulent patches in the ocean thermocline (Smyth et al., 2001).

OCEANIC OBSERVATIONS OF KH INSTABILITY AND THE TRANSITION TO TURBULENCE

We next describe two examples of turbulence arising from KH billows in disparate geographical locations and governed by very different internal wave

dynamics. The first comes from the interior of large-amplitude (and nonlinear) internal waves on the continental shelf. In waters that are relatively devoid of small fish and zooplankton, the principal source of acoustic backscatter at 120 kHz is the density and sound speed microstructure created by turbulence, a point made clear by broadband acoustic measurements through these waves that reveal the full spectrum of the backscattering that permits discrimination between zooplankton and turbulence (Lavery et al., 2010). In Figure 8, acoustic backscattering illuminates a train of billows with dimensions similar to those seen over Great Meteor Seamount (Figure 4 and accompanying text), but here embedded within a wave propagating toward the Oregon coast (Moum et al., 2003). The sequence of rollups is identical in nature to Kelvin-Helmholtz instabilities observed in the laboratory and in small-scale simulations (Figures 2 and 7). The vertical scale of the largest

rollup is more than 10 m, and the horizontal scale (in the direction of wave propagation) is roughly 50 m. Toward the trailing edge of the wave, the rollups become less coherent but contribute a greater backscatter signal, indicating breakdown to turbulence. The turbulent region between the two largest billows suggests the braid-centered secondary instability of Mashayek and Peltier (2011). At greater depth, denoted by arrows, are two more layers of bright backscatter. They are presumably the same phenomenon, but smaller scale; if so, the echosounder resolution does not permit a clear depiction of these deeper rollups. The bright acoustic scattering tail of large-amplitude internal waves is a common feature on continental shelves.

The second example is from the upper equatorial ocean. The signature equatorial current structure in the upper 150 m of the central Pacific includes a strong westward surface current overlying an equally intense eastward undercurrent.

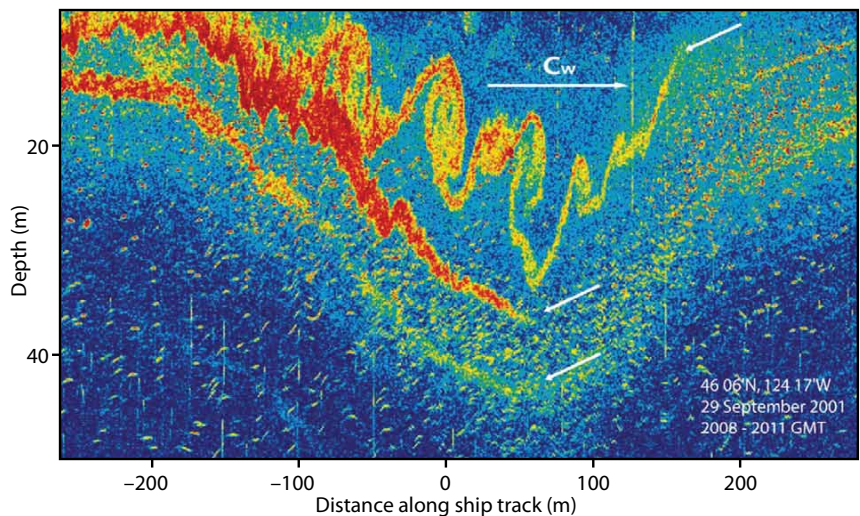


Figure 8. Example acoustical snapshot of a nonlinear internal gravity wave approaching the Oregon coast. The wave propagates from left to right at speed C_w in this image. The velocity in the upper layer is in the direction of C_w , and the resultant current shear defines the direction of the rollups in the billows. The bright acoustic scattering layers result from reflections by density microstructure caused by turbulence. The signal reveals a train of Kelvin-Helmholtz billows. The structure located between the two largest billows may be an example of the stagnation point instability (Mashayek and Peltier, 2011).

As a result, current shear is large and, despite strong stratification, Ri is typically near-critical in the mean.³ It has long been suspected that turbulence generated beneath the equatorial mixed layer (which does not generally extend as far as it does beneath mid-latitude mixed layers) is due to shear instability. Recent measurements from a vertical array of fast temperature sensors moored for extended periods in the upper equatorial ocean have confirmed the basic structure of KH instability in the small-scale fluctuations that appear on a daily cycle at frequencies near the local buoyancy frequency, N (Figure 9; Moum et al., 2011). The frequency and intermittency of the fluctuations can be seen in the Figure 9a spectrogram. The

phase of the oscillations varies vertically in a manner consistent with KH instability. Oscillations typically comprise $O(10)$ wavelengths. Potential energy stored in these motions (Figure 9b) also varies on a daily basis and is correlated with the turbulent kinetic energy dissipation rate (Figure 9c), indicating that turbulent mixing at small scales coincides with KH billows (Figure 9d).

The interpretation of these fluctuations as KH billows has been tested via application to oceanic data of Rayleigh's (1880) method of linear stability analysis. That method has been used in the interpretation of billows observed in the atmosphere (Busack and Brummer, 1988) and in the ocean (Mack and Hebert, 1997; Sun et al., 1998), and is

now used routinely in data analysis. Linear stability analysis provides compelling evidence that the oscillations found in strongly sheared equatorial currents are, in fact, a KH instability. Predicted wavelengths of computed instabilities (Sun et al., 1998; Figure 10a) agree with directly measured wavelengths (Moum et al., 1992), and predicted frequencies (Smyth et al., 2011; Figure 10b) also agree well with directly measured frequencies (Moum et al., 2011). These analyses show that the conditions for the growth of KH instability occur sporadically, which in turn suggests that random internal wave interactions add to the ambient shear to drive Ri to subcritical values, thereby generating instability at random points in space and time. The similarity between the dominant frequency of the oscillations and N is consistent with this scenario, even though the frequency of individual KH events is independent of stratification (see Box 1).

The relationship between KH instability and small-scale turbulence is complex: the instability causes turbulence, and turbulence already present in the environment affects its growth. Liu et al. (2011) have recently extended the classical method of stability analysis to include the effects of ambient turbulence. In strongly forced flows, such as exist in the upper equatorial ocean, this relationship can lead to a cycle in which shear is continually reinforced, but new instabilities cannot grow until turbulence generated by previous instabilities decays.

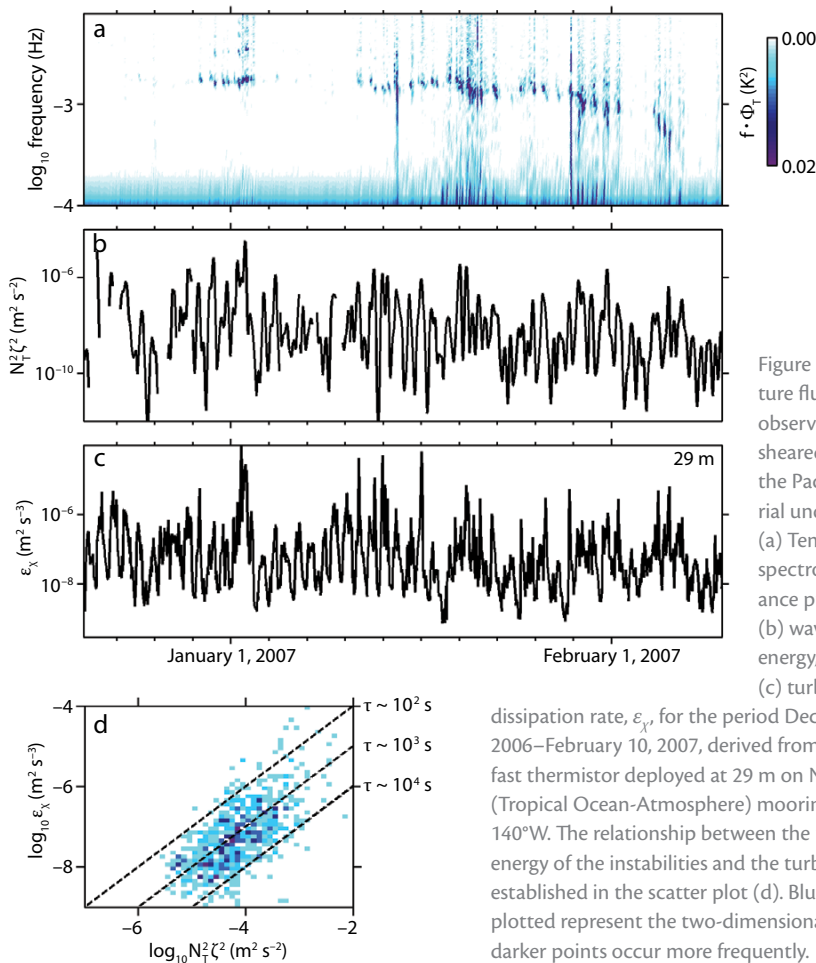


Figure 9. Temperature fluctuations observed in the sheared zone above the Pacific equatorial undercurrent. (a) Temperature spectrogram (variance preserving), (b) wave potential energy, $N^2 \zeta^2$, and (c) turbulence

dissipation rate, ϵ_x , for the period December 20, 2006–February 10, 2007, derived from a single fast thermistor deployed at 29 m on NOAA's TAO (Tropical Ocean-Atmosphere) mooring at 0°, 140°W. The relationship between the potential energy of the instabilities and the turbulence is established in the scatter plot (d). Blue points plotted represent the two-dimensional histogram; darker points occur more frequently.

³ In the case of large-amplitude internal waves, the shear at a point in space is short-lived, and so also is near-critical Ri . The important issue of how long near-critical Ri must persist for instability to occur has been examined in laboratory and numerical experiments (Fructus et al., 2009; Inoue and Smyth, 2009; Barad and Fringer, 2010).

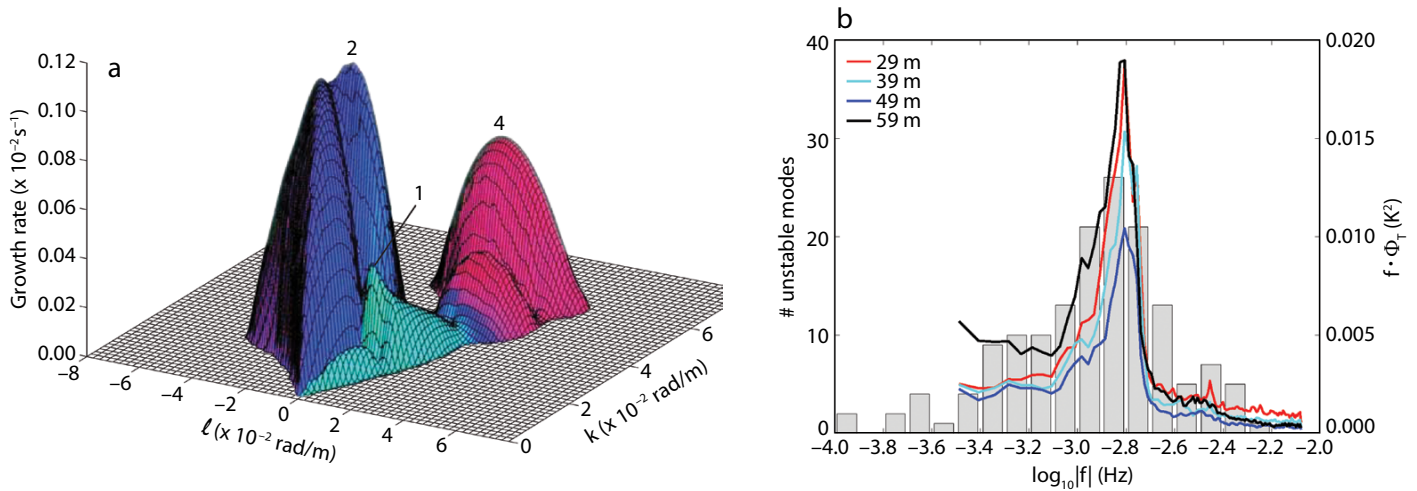


Figure 10. Linear stability analyses of flow above the Pacific equatorial undercurrent. (a) Growth rate versus zonal and meridional wavenumbers. Colors represent mode families focused in different shear layers between the undercurrent core and the surface (Sun et al., 1998). *Graphic courtesy C. Sun.* (b) Histogram of absolute cyclic frequency for 155 unstable modes computed numerically from hourly averaged profiles of velocity and density (Smyth et al., 2011). Curves show normalized, variance-preserving spectra of four observed temperature time series. Sensor depths are as shown in the legend.

BOX 1 | WHY KELVIN-HELMHOLTZ BILLOWS ARE NEAR- N

Oscillations in the upper equatorial Pacific, thought to arise from KH instability, show a striking tendency to have frequency close to N , the buoyancy frequency. This is not a property of individual KH billows, but may follow from the statistics of a random ensemble of instabilities due to sporadic shear amplification by interacting gravity waves.

Consider a random ensemble of instabilities growing on small shear layers within a larger sheared zone. Phase velocities lie approximately within the range of the mean current (Howard, 1961; Figure B1), $U_{min} < c < U_{max}$. The observer's velocity is assumed to lie in the range of the mean flow, so that $U_{min} < 0$ and $U_{max} > 0$. Wavelengths lie between zero and about seven times the thickness of the largest shear layer (e.g., Hazel, 1972; Figure B2).

Treating phase velocity and wavelength as independent random variables yields a probability distribution function for the frequency (Figure B3), shown in blue for representative values $U_{min} = -1 \text{ ms}^{-1}$, $U_{max} = 1 \text{ ms}^{-1}$, and $\lambda_0 = 700 \text{ m}$. For comparison, gray bars show the frequency distribution of instabilities computed via linear stability analysis of the observed velocity and density profiles. The theoretical peak frequency, $f_{peak} = \max(|U_{min}|, U_{max})/\lambda_0$ is consistent with that of computed instabilities for this regime, and also with observations (Figure 10).

Given that the maximum possible wavelength λ_0 is about 2π times the thickness D of the sheared zone, the peak angular frequency $\omega_{peak} = 2\pi f_{peak}$ is within a factor two of the mean shear. (Since $U_{min} < 0$, the mean shear would be $(U_{max} + |U_{min}|)/D$, and the sum of two positive numbers is, at most, twice the greater.) The mean flow is characterized by Richardson number of order unity, hence N and the shear are nearly equal, implying that $\omega_{peak} \sim N$.

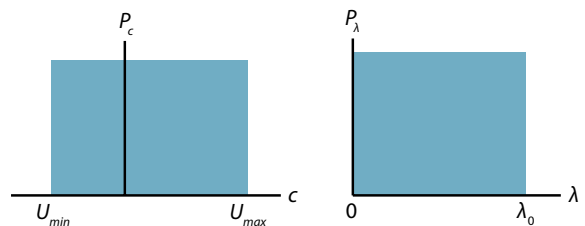


Figure B1. Probability distribution of phase velocity.

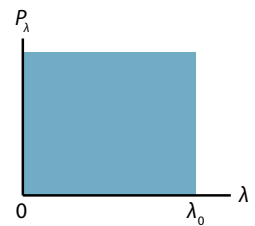


Figure B2. Probability distribution of wavelength.

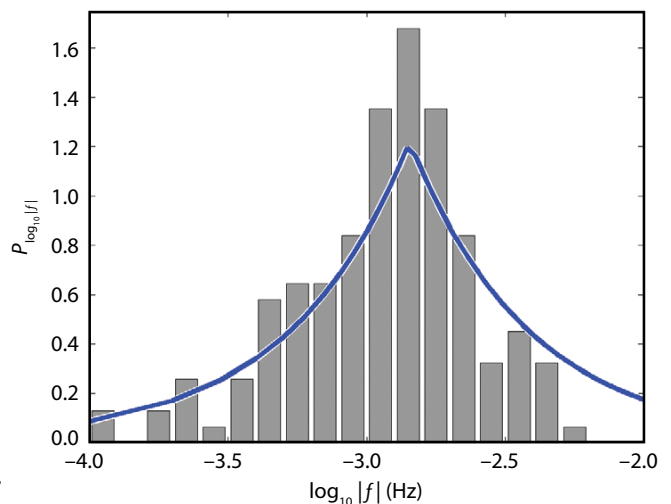



Figure B3. Probability distribution function for the frequency: theoretical (blue) and based on linear stability analysis of measured flows (gray).

QUANTIFYING MIXING BY KH INSTABILITY

To determine the net contribution of KH instability to global mixing, two critical challenges must be addressed. The first is to quantify the prevalence of KH instability in thermocline internal wave fields. Other forms of instability contribute to thermocline mixing. How much? One way this quantity is being measured is with long time series that include sufficient detail to diagnose KH instability in the signal such as those made in the upper equatorial ocean by Moum et al. (2011; Figure 9). Can thermocline observations with the same fidelity be obtained that permit an evaluation of the prevalence of KH instability in thermocline internal wave fields? Glider measurements are promising in this respect (e.g., Thorpe 2012; Smyth and Thorpe 2012.)

The second challenge is to parameterize KH-induced mixing (i.e., to approximate the rate of mixing in terms of other quantities that are more easily measured or modeled). For example, Kunze et al. (1990) used a simple analytical model of a shear layer to estimate the mean flow kinetic energy released in an instability event and combined the result with an estimate of the turbulence production time to arrive at the kinetic energy dissipation rate. Future parameterizations will incorporate more complete models of instability physics, and they will be calibrated using advanced laboratory techniques, comprehensive microstructure observations, and direct numerical simulations of increasing scale and realism.

ACKNOWLEDGEMENTS

Our work on KH instability has been funded by the National Science Foundation (1030772 and 1129419 to WDS, and 0728357 and 1059055 to JNM) and by the Office of Naval Research (N00014-09-1-0280, N00014-10-1-2098 to JNM). Helpful critiques of this article were provided by Steve Thorpe, Aurelie Moulin, Elizabeth McHugh and two anonymous referees. 

REFERENCES

- Baines, P.G., and H. Mitsudera. 1994. On the mechanism of shear flow instabilities. *Journal of Fluid Mechanics* 276:327–342, <http://dx.doi.org/10.1017/S0022112094002582>.
- Barad, M.F., and O.B. Fringer. 2010. Simulations of shear instabilities in interfacial gravity waves. *Journal of Fluid Mechanics* 644:61–95, <http://dx.doi.org/10.1017/S0022112009992035>.
- Busack, B., and B. Brummer. 1988. A case study of Kelvin-Helmholtz waves within an offshore stable boundary layer: Observations and linear model. *Boundary-Layer Meteorology* 44:105–135, <http://dx.doi.org/10.1007/BF00117295>.
- Caulfield, C.P., and W.R. Peltier. 1994. Three-dimensionalization of the stratified mixing layer. *Physics of Fluids A* 6(12):3,803–3,805, <http://dx.doi.org/10.1063/1.868370>.
- Corcos, G., and F. Sherman. 1976. Vorticity concentration and the dynamics of unstable free shear layers. *Journal of Fluid Mechanics* 73: 241–264, <http://dx.doi.org/10.1017/S0022112076001365>.
- Dunkerton, T. 1997. Shear instability of internal inertia-gravity waves. *Journal of the Atmospheric Sciences* 54:1,628–1,641, [http://dx.doi.org/10.1175/1520-0469\(1997\)054<1628:SIOIIG>2.0.CO;2](http://dx.doi.org/10.1175/1520-0469(1997)054<1628:SIOIIG>2.0.CO;2).
- Fructus, D., M. Carr, J. Grue, A. Jensen, and P.A. Davies. 2009. Shear-induced breaking of large internal solitary waves. *Journal of Fluid Mechanics* 620:1–29, <http://dx.doi.org/10.1017/S0022112008004898>.
- Geyer, W.R., A. Lavery, M.E. Scully, and J.H. Trowbridge. 2010. Mixing by shear instability at high Reynolds number. *Geophysical Research Letters* 37, L22607, <http://dx.doi.org/10.1029/2010GL045272>.
- Geyer, W.R., and J.D. Smith. 1987. Shear instability in a highly stratified estuary. *Journal of Physical Oceanography* 17:1,668–1,679, [http://dx.doi.org/10.1175/1520-0485\(1987\)017<1668:SIIAHS>2.0.CO;2](http://dx.doi.org/10.1175/1520-0485(1987)017<1668:SIIAHS>2.0.CO;2).

- Goldstein, S. 1931. On the stability of superposed streams of fluids of different densities. *Proceedings of the Royal Society of London A* 132:524–548, <http://dx.doi.org/10.1098/rspa.1931.0116>.
- Gregg, M.C. 1989. Scaling turbulent dissipation in the thermocline. *Journal of Geophysical Research* 94:9,686–9,698, <http://dx.doi.org/10.1029/JC094iC07p09686>.
- Hazel, P. 1972. Numerical studies of the stability of inviscid stratified shear flows. *Journal of Fluid Mechanics* 51:39–61, <http://dx.doi.org/10.1017/S0022112072001065>.
- Henye, F.S., J. Wright, and S.M. Flatté. 1986. Energy and action flow through the internal wave field: An eikonal approach. *Journal of Geophysical Research* 91(C7):8,487–8,495, <http://dx.doi.org/10.1029/JC091iC07p08487>.
- Hibiya, T., Y. Niwa, and K. Fujiwara. 1998. Numerical experiments of nonlinear energy transfer within the oceanic internal wave spectrum. *Journal of Geophysical Research* 103(C9):18,715–18,722, <http://dx.doi.org/10.1029/98JC01362>.
- Howard, L.N. 1961. Note on a paper of John W. Miles. *Journal of Fluid Mechanics* 10:509–512, <http://dx.doi.org/10.1017/S0022112061000317>.
- Inoue, R., and W.D. Smyth. 2009. Efficiency of mixing forced by unsteady shear flow. *Journal of Physical Oceanography* 39:1,150–1,166, <http://dx.doi.org/10.1175/2008JPO3927.1>.
- Kimura, S., and W.D. Smyth. 2007. Direct numerical simulation of salt sheets and turbulence in a double-diffusive shear layer. *Geophysical Research Letters* 34, L21610, <http://dx.doi.org/10.1029/2007GL031935>.
- Klaassen, G.P., and W.R. Peltier. 1985. The evolution of finite-amplitude Kelvin-Helmholtz billows in two spatial dimensions. *Journal of the Atmospheric Sciences* 42:1,321–1,339, [http://dx.doi.org/10.1175/1520-0469\(1985\)042<1321:EOFAKB>2.0.CO;2](http://dx.doi.org/10.1175/1520-0469(1985)042<1321:EOFAKB>2.0.CO;2).
- Klaassen, G.P., and W.R. Peltier. 1991. The influence of stratification on secondary instability in free shear layers. *Journal of Fluid Mechanics* 227:71–106, <http://dx.doi.org/10.1017/S0022112091000046>.
- Kunze, E., A.J. Williams III, and M.G. Briscoe. 1990. Observations of shear and vertical stability from a neutrally buoyant float. *Journal of Geophysical Research* 95:18,127–18,142, <http://dx.doi.org/10.1029/JC095iC10p18127>.
- Lamb, K.G., and D. Farmer. 2011. Instabilities in an internal solitary-like wave on the Oregon shelf. *Journal of Physical Oceanography* 41:67–87, <http://dx.doi.org/10.1175/2010JPO4308.1>.
- Lavery, A.C., D. Chu, and J.N. Moum. 2010. Observations of broadband acoustic backscattering from nonlinear internal waves: Assessing the contribution from microstructure. *IEEE Journal of Ocean Engineering* 35:695–709, <http://dx.doi.org/10.1109/JOE.2010.2047814>.
- Lelong, M.-P., and T.J. Dunkerton. 1998a. Inertia-gravity wave breaking in three dimensions. Part I: Convectively stable waves. *Journal*

- of the *Atmospheric Sciences* 55:2,473–2,488, [http://dx.doi.org/10.1175/1520-0469\(1998\)055<2473:IGWBIT>2.0.CO;2](http://dx.doi.org/10.1175/1520-0469(1998)055<2473:IGWBIT>2.0.CO;2).
- Lelong, M.-P., and T.J. Dunkerton. 1998b. Inertia-gravity wave breaking in three dimensions. Part II: Convectively unstable waves. *Journal of the Atmospheric Sciences* 55:2,489–2,501, [http://dx.doi.org/10.1175/1520-0469\(1998\)055<2489:IGWBIT>2.0.CO;2](http://dx.doi.org/10.1175/1520-0469(1998)055<2489:IGWBIT>2.0.CO;2).
- Liu, Z., S.A. Thorpe, and W.D. Smyth. 2011. Instability and hydraulics of turbulent stratified shear flows. *Journal of Fluid Mechanics* 695:235–256, <http://dx.doi.org/10.1017/jfm.2012.13>.
- Mack, A., and D. Hebert. 1997. Internal gravity waves in the upper eastern equatorial Pacific: Observations and numerical solutions. *Journal of Geophysical Research* 102:21,081–21,100, <http://dx.doi.org/10.1029/97JC01506>.
- Mashayek, A., and W.R. Peltier. 2011. Three-dimensionalization of the stratified mixing layer at high Reynolds number. *Physics of Fluids* 23, 111701, <http://dx.doi.org/10.1063/1.3651269>.
- Mellor, G., and T. Yamada. 1982. Development of a turbulence closure model for geophysical applications. *Reviews of Geophysics* 20(4):851–875, <http://dx.doi.org/10.1029/RG020i004p00851>.
- Miles, J.W. 1961. On the stability of heterogeneous shear flows. *Journal of Fluid Mechanics* 10:496–508, <http://dx.doi.org/10.1017/S0022112061000305>.
- Moum, J.N., D.M. Farmer, W.D. Smyth, L. Armi, and S. Vagle. 2003. Structure and generation of turbulence at interfaces strained by internal solitary waves propagating shoreward over the continental shelf. *Journal of Physical Oceanography* 33:2,093–2,122, [http://dx.doi.org/10.1175/1520-0485\(2003\)033<2093:SAGOTA>2.0.CO;2](http://dx.doi.org/10.1175/1520-0485(2003)033<2093:SAGOTA>2.0.CO;2).
- Moum, J.N., D. Hebert, C.A. Paulson, and D.R. Caldwell. 1992. Turbulence and internal waves at the equator. Part I: Statistics from towed thermistors and a microstructure profiler. *Journal of Physical Oceanography* 22:1,330–1,345, [http://dx.doi.org/10.1175/1520-0485\(1992\)022<1330:TAIWAT>2.0.CO;2](http://dx.doi.org/10.1175/1520-0485(1992)022<1330:TAIWAT>2.0.CO;2).
- Moum, J.N., J.D. Nash, and W.D. Smyth. 2011. Narrowband oscillations in the upper equatorial ocean. Part I: Interpretation as shear instabilities. *Journal of Physical Oceanography* 41:397–411, <http://dx.doi.org/10.1175/2010JPO4450.1>.
- Patnaik, P., F.S. Sherman, and G.M. Corcos. 1976. A numerical simulation of Kelvin-Helmholtz waves of finite amplitude. *Journal of Fluid Mechanics* 73:215–240, <http://dx.doi.org/10.1017/S0022112076001353>.
- Polzin, K.L. 1996. Statistics of the Richardson number: Mixing models and finestructure. *Journal of Physical Oceanography* 26:1,409–1,425, [http://dx.doi.org/10.1175/1520-0485\(1996\)026<1409:SOTRNM>2.0.CO;2](http://dx.doi.org/10.1175/1520-0485(1996)026<1409:SOTRNM>2.0.CO;2).
- Polzin, K.L., J.M. Toole, and R.W. Schmitt. 1995. Finescale parameterizations of turbulent dissipation. *Journal of Physical Oceanography* 25:306–328, [http://dx.doi.org/10.1175/1520-0485\(1995\)025<0306:FPOTD>2.0.CO;2](http://dx.doi.org/10.1175/1520-0485(1995)025<0306:FPOTD>2.0.CO;2).
- Price, J.F., R.A. Weller, and R. Pinkel. 1986. Diurnal cycling: Observations and models of the upper ocean response to diurnal heating, cooling and wind mixing. *Journal of Geophysical Research* 91(C7):8,411–8,427, <http://dx.doi.org/10.1029/JC091iC07p08411>.
- Rayleigh, L. 1880. On the stability or instability of certain fluid motions. *Proceedings of the London Mathematical Society* 11:57–70, <http://dx.doi.org/10.1112/plms/s1-11.1.57>.
- Reynolds, O. 1883. An experimental investigation of the circumstances which determine whether the motion of water shall be direct or sinuous, and of the law of resistance in parallel channels. *Philosophical Transactions of the Royal Society* 174:935–982.
- Scinocca, J.F. 1995. The mixing of mass and momentum by Kelvin-Helmholtz billows. *Journal of the Atmospheric Sciences* 52:2,509–2,530.
- Smyth, W.D. 1999. Dissipation range geometry and scalar mixing in sheared, stratified turbulence. *Journal of Fluid Mechanics* 401:209–242.
- Smyth, W.D. 2003. Secondary Kelvin-Helmholtz instability in weakly stratified shear flow. *Journal of Fluid Mechanics* 497:67–98, <http://dx.doi.org/10.1017/S0022112003006591>.
- Smyth, W.D., and S. Kimura. 2011. Mixing in a moderately sheared salt fingering layer. *Journal of Physical Oceanography* 41:1,361–1,381, <http://dx.doi.org/10.1175/2010JPO4611.1>.
- Smyth, W.D., J.N. Moum, and D.R. Caldwell. 2001. The efficiency of mixing in turbulent patches: Inferences from direct simulations and microstructure observations. *Journal of Physical Oceanography* 31:1,969–1,992, [http://dx.doi.org/10.1175/1520-0485\(2001\)031<1969:TEOMIT>2.0.CO;2](http://dx.doi.org/10.1175/1520-0485(2001)031<1969:TEOMIT>2.0.CO;2).
- Smyth, W.D., J.N. Moum, and J.D. Nash. 2011. Narrowband oscillations in the upper equatorial ocean. Part II: Properties of shear instabilities. *Journal of Physical Oceanography* 41:412–428, <http://dx.doi.org/10.1175/2010JPO4451.1>.
- Smyth, W.D., and S.A. Thorpe. 2012. Glider measurements of overturning in a Kelvin-Helmholtz billow train. *Journal of Marine Research* 70:117–140.
- Staquet, C. 1995. Two-dimensional secondary instabilities in a strongly stratified shear layer. *Journal of Fluid Mechanics* 296:73–126, <http://dx.doi.org/10.1017/S0022112095002072>.
- Stern, M.E. 1969. Collective instability of salt fingers. *Journal of Fluid Mechanics* 35:209–218, <http://dx.doi.org/10.1017/S0022112069001066>.
- Sun, C., W.D. Smyth, and J.N. Moum. 1998. Dynamic instability of stratified shear flow in the upper equatorial Pacific. *Journal of Geophysical Research* 103(C5):10,323–10,337, <http://dx.doi.org/10.1029/98JC00191>.
- Taylor, G.I. 1927. An experiment on the stability of superposed streams of fluid. *Proceedings of the Cambridge Philosophical Society* 23:730–731, <http://dx.doi.org/10.1017/S0305004100011245>.
- Taylor, G.I. 1931. Effect of variation in density on the stability of superposed streams of fluid. *Proceedings of the Royal Society of London* 132:499–523, <http://dx.doi.org/10.1098/rspa.1931.0115>.
- Thomson, W. (Lord Kelvin). 1871. Hydrokinetic solutions and observations. *Philosophical Magazine* 42:362–377.
- Thorpe, S.A. 1969. Neutral eigensolutions of the stability equation for stratified shear flow. *Journal of Fluid Mechanics* 36:673–683, <http://dx.doi.org/10.1017/S0022112069001923>.
- Thorpe, S.A. 1971. Experiments on the instability of stratified shear flows: Miscible fluids. *Journal of Fluid Mechanics* 46:299–319, <http://dx.doi.org/10.1017/S0022112071000557>.
- Thorpe, S.A. 1985. Laboratory observations of secondary structures in Kelvin-Helmholtz billows and consequences for ocean mixing. *Geophysical and Astrophysical Fluid Dynamics* 34:175–199.
- Thorpe, S.A. 1987. Transition phenomena and the development of turbulence in stratified fluids. *Journal of Geophysical Research* 92(C5):5,231–5,245, <http://dx.doi.org/10.1029/JC092iC05p05231>.
- Thorpe, S.A. 2002. The axial coherence of Kelvin-Helmholtz billows. *Quarterly Journal of the Royal Meteorological Society* 128:1,529–1,542, <http://dx.doi.org/10.1002/qj.200212858307>.
- Thorpe, S.A. 2012. Measuring overturns with gliders. *Journal of Marine Research* 70:93–117.
- van Haren, H., and L. Gostiaux. 2010. A deep-ocean Kelvin-Helmholtz billow train. *Geophysical Research Letters* 37, L03605, <http://dx.doi.org/10.1029/2009GL041890>.
- Venayagamoorthy, S.K., and O.B. Fringer. 2012. Examining breaking internal waves on a shelf slope using numerical simulations. *Oceanography* 25(2):132–139, <http://dx.doi.org/10.5670/oceanog.2012.48>.
- von Helmholtz, H. 1890. Die energie der wogen und des windes. *Annalen der Physik* 41:641–662, <http://dx.doi.org/10.1002/andp.18902771202>.
- Wesson, J.C., and M.C. Gregg. 1994. Mixing at Camarinal Sill in the Strait of Gibraltar. *Journal of Geophysical Research* 99(C5):9,847–9,878, <http://dx.doi.org/10.1029/94JC00256>.
- Woods, J.D. 1968. Wave-induced shear instability in the summer thermocline. *Journal of Fluid Mechanics* 32:791–800, <http://dx.doi.org/10.1017/S0022112068001035>.